JGR Oceans

RESEARCH ARTICLE
10.1029/2018JC014735

Interannual Coral $\Delta^{14}C$ Records of Surface Water Exchange Across the Luzon Strait

R. D. Ramos[1], N. F. Goodkin[1,2,3], E. R. M. Druffel[4], T. Y. Fan[5], and F. P. Siringan[6]

[1]Asian School of the Environment, Nanyang Technological University, Singapore, [2]Earth Observatory of Singapore, Nanyang Technological University, Singapore, [3]American Museum of Natural History, New York, NY, USA, [4]Department of Earth System Science, University of California, Irvine, CA, USA, [5]National Museum of Marine Biology and Aquarium, Pingtung, Taiwan, R.O.C, [6]The Marine Science Institute, University of the Philippines Diliman, Quezon City, Philippines

Key Points:
- Early bomb-produced ^{14}C spikes are evident in the Luzon Strait $\Delta^{14}C$ records
- Interannual differences between our sites and other $\Delta^{14}C$ records reveal basin-specific processes controlling regional $\Delta^{14}C$ variability
- ENSO mainly drives the mean transport across the strait

Supporting Information:
- Supporting Information S1
- Data Set S1
- Data Set S2

Correspondence to:
R. D. Ramos,
ramo0002@ntu.edu.sg

Citation:
Ramos, R. D., Goodkin, N. F., Druffel, E. R. M., Fan, T. Y., & Siringan, F. P. (2019). Interannual coral $\Delta^{14}C$ records of surface water exchange across the Luzon Strait. *Journal of Geophysical Research: Oceans*, *124*, 491–505. https://doi.org/10.1029/2018JC014735

Received 3 NOV 2018
Accepted 23 DEC 2018
Accepted article online 2 JAN 2019
Published online 21 JAN 2019

Abstract The Luzon Strait (LS) hosts the largest transport of water between the Western Pacific Ocean (WPO) and the South China Sea (SCS). The transport through the strait, dominated by the westward propagation of the Kuroshio Intrusion, influences the climate and circulation of the SCS. While numerical models have investigated the interannual variability of the transport and subsequent water exchange across the LS, a lack of long-term on-site records prevents a general consensus on the transport rates, variability, and drivers. Corals offer high-resolution, continuous histories of radiocarbon ($\Delta^{14}C$) content of the seawater dissolved inorganic carbon, allowing us to track changes in ocean transport and circulation through time. Seasonal and annual $\Delta^{14}C$ samples from Houbihu, Taiwan, and Palaui, Philippines, located on either side of the strait, are compared to the Western Pacific Ocean and SCS $\Delta^{14}C$ records to examine the spatial and temporal $\Delta^{14}C$ variability in the region. We calculated the mean transport across the strait using a five-box mixing model and identified its potential drivers. The mean amount of water exchanged across the strait from 1970 to 1999 was 2.2 Sv, ranging from −13.4 to 16 Sv, where a positive (negative) value indicates net flow into (out of) the SCS. A weaker East Asian Winter Monsoon increases the contribution of the SCS outflow on the Kuroshio Intrusion-dominated LS, while the El Niño–Southern Oscillation primarily drives the intrusion into the SCS. These results provide support to the dominant control of El Niño–Southern Oscillation on the long-term ocean circulation variability in this region.

Plain Language Summary The Luzon Strait is a globally critical ocean pathway that links the Western Pacific Ocean and the South China Sea (SCS). Heat, salt, and nutrients are exchanged across the strait, impacting marine ecology and climate in the region. In situ measurements of the surface water processes across the strait are limited, complicating our understanding of its variability and driving mechanism. Here, we present radiocarbon measurements, which represent a record of surface ocean processes including upwelling, extending beyond the instrumental record using two corals collected from either side of the strait, Houbihu, Taiwan, and Palaui, Philippines. Houbihu is impacted by the strength of the East Asian Winter Monsoon winds, affecting the transport of surface waters into and out of the SCS. Palaui is sensitive to surface transports linked to the shifts of the North Equatorial Current bifurcation latitude, primarily influenced by the El Niño–Southern Oscillation. While different processes impact our sites, the difference in the amount of radiocarbon between Houbihu and Palaui and the surrounding seas allows us to further investigate changes to water exchange across the strait. We find that a weaker East Asian Winter Monsoon impedes water inflow into the SCS whereas El Niño–Southern Oscillation facilitates inflow into the SCS.

1. Introduction

The Luzon Strait (LS), ~350 km wide with a sill depth of ~2,500 m, is the widest and deepest channel surrounding the South China Sea (SCS) and thus provides the largest exchange between the Western Pacific Ocean (WPO) and the SCS (Figure 1; C.-T. Chen et al., 2015; Jia & Chassignet, 2011; Liang et al., 2008; Metzger & Hurlburt, 2001; Nan et al., 2015; Peñaflor et al., 2007). The northward flowing Kuroshio Current (KC) periodically intrudes through the strait into the SCS as the Kuroshio Intrusion (KI), significantly contributing to mean Luzon Strait Transport (LST; Caruso et al., 2006; Centurioni et al., 2004; J. Hu et al., 2000; Jia & Liu, 2004; Nan et al., 2015; Wyrtki, 1961). The KI delivers warmer and more saline waters from the WPO into the SCS, regulating heat, moisture, and water exchange along its path

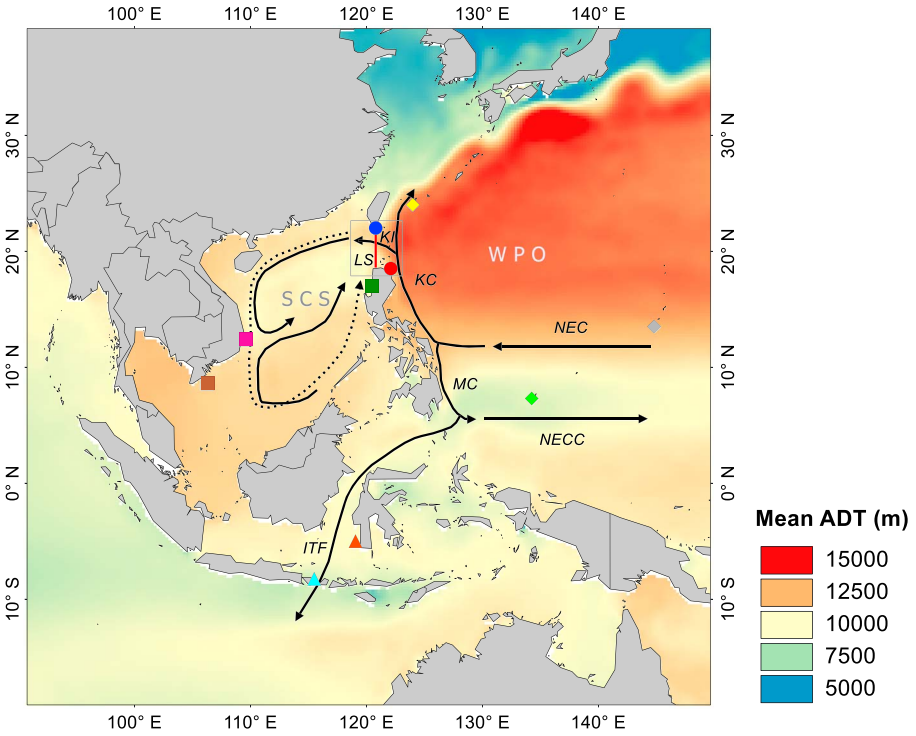

Figure 1. Mean absolute dynamic topography (ADT, 1993–2017) over the western Pacific region derived from the Archiving, Validation, and Interpolation of Satellite Oceanographic data (http://www.aviso.altimetry.fr/duacs/). Gray box marks the Luzon Strait (LS). Black solid and dotted lines delineate the general ocean circulation pattern over the WPO (Hu et al., 2015; Qiu & Lukas, 1996), the SCS (dotted lines are during winter, solid lines are during summer; P.-X. Wang & Li, 2009), and the ITF (Gordon et al., 2012). Colored symbols indicate the location of coral $\Delta^{14}C$ records used in this study: blue circle = Houbihu, Taiwan and red circle = Palaui, Philippines (this study); gray diamond = Guam, USA (Andrews et al., 2016); light green diamond = Palau (Glynn et al., 2013); yellow diamond = Ishigaki Island, Japan (Hirabayashi, Yokoyama, Suzuki, Miyairi, & Aze, 2017); orange triangle = Langkai, Indonesia (Fallon & Guilderson, 2008); light blue triangle = Lombok Strait, Indonesia (Guilderson et al., 2009); green square = Currimao, Philippines (Hirabayashi, Yokoyama, Suzuki, Miyairi, Aze, Siringan, & Maeda, 2017); pink square = Hon Tre, Vietnam (Bolton et al., 2016); and brown square = Con Dao, Vietnam (Mitsuguchi et al., 2007). The red line across the strait at 120.8°E running from 18°N to 22°N define the transect where surface zonal currents and sea surface heights from the Simple Ocean Data Assimilation data set (SODA v.2.2.4, http://apdrc.soest.hawaii.edu/dods/public_data/SODA/soda_pop2.2.4) are derived (shown in Figures 3 and 4c, respectively). NEC = North Equatorial Current; NECC = North Equatorial Counter Current; KC = Kuroshio Current; KI = Kuroshio Intrusion; MC = Mindanao Current; SCS = South China Sea; WPO = Western Pacific Ocean; ITF = Indonesian Throughflow.

(Caruso et al., 2006; C.-T. Chen et al., 2001; D. Hu et al., 2015; Nan et al., 2015; Qiu & Lukas, 1996). SCS outflow crosses the LS toward the WPO at lower rate, causing water and nutrient exchange along the strait (Chern & Wang, 1998; Du et al., 2013; Hsin et al., 2012; Qu et al., 2004; Xue et al., 2004).

Intermittent measurements and multiyear hydrographic observations of the water exchange across the strait reveal a spatially variable structure of the LST. The mean transport across the strait has a sandwich-like vertical structure, such that the upper (i.e., <500 m) and deep (i.e., 1,500 m) layers flow into the SCS and the middle layer (i.e., 500 to 1,500 m) flows out to the WPO (Nan et al., 2015; Qu et al. 2006, 2000; Shaw & Chao, 1994; Tian et al., 2006). In the upper layers (i.e., 0 to 300 m), eastward and westward currents are also observed to alternate spatially. Inflow to the SCS is commonly observed across 19.5–21°N (G. Chen, Hou, & Chu, 2011; Hsin et al., 2012; Liang et al., 2008; Xue et al., 2004) and the direction typically reverses north of 21°N (G. Chen, Hou, & Chu, 2011; Hsin et al., 2012; Liang et al., 2008; Nan et al., 2015; Xue et al., 2004). The net flow into the SCS varies between 3 and 6.5 Sv (1 Sv = 10^6 m^3/s) annually (Nan et al., 2015). The LST also shows strong monsoon-driven seasonal variation, where maximum intrusions (minimal outflows) of 2.75 to 13.7 Sv (0.2 to 2.75 Sv) occur during winter (summer) when the northeast (southwest) monsoon predominates (Centurioni et al., 2004; G. Chen, Hu, et al., 2011; Hsin et al., 2012; Metzger & Hurlburt, 1996; Nan et al., 2015; Qu et al., 2004, 2000; Tian et al., 2006; Wyrtki, 1961; Yang et al., 2010; Yaremchuk & Qu, 2004). Numerical models are able to reproduce similar spatial and temporal variability but further magnify quantitative inconsistencies in the observed mean transport. Model-derived LST estimates (e.g., Hsin et al., 2012; Nan et al., 2015) indicate a mean westward transport of 0.6 to 10.2 Sv, while seasonal transports vary

from 3.1 to 12.2 Sv and 0.7 to 8.2 Sv for winters and summers, respectively. The large range of these estimates primarily result due to the differences in the methodology and model assumptions (Hsin et al., 2012; Nan et al., 2015).

Compared to seasonal variability, the interannual LST variation and its controlling mechanisms are less understood due to scarcity of continuous direct observations (Nan et al., 2015; Wu, 2013). Numerical models show that the El Niño–Southern Oscillation (ENSO) exerts influence on the interannual variability of the LST by means of shifting the position of the North Equatorial Current (NEC) bifurcation latitude (e.g., Qu et al., 2004). The position of the bifurcation latitude determines the volume of the Kuroshio relative to the southward flowing Mindanao Current (MC) and the subsequent intrusion into the SCS. During El Niño years, anomalous southerly winds east of the Philippines push the bifurcation latitude northward reducing the Kuroshio transport east of Luzon (Y. Y. Kim et al., 2004; Qiu & Chen, 2010; Qiu & Lukas, 1996; Q.-Y. Wang & Hu, 2006) and increasing the KI into the SCS potentially a result of inertial effects (Gordon et al., 2014; Qu et al., 2004; Yaremchuk & Qu, 2004). The situation then reverses for La Niña periods. However, recent studies show that the interannual variability of the NEC bifurcation and, consequently, the mean flow across the strait is strongly linked to the Pacific Decadal Oscillation (PDO) and not ENSO (e.g., Nan et al., 2016; Wu, 2013; Wu et al., 2016). With the more frequent PDO shifts in the recent years, ENSO is hypothesized to exert less impact on the NEC bifurcation latitude migration and mean LST, especially after 1995 when the PDO became predominantly negative (Wu, 2013). Similar to the ENSO-related wind forcing, anomalous winds during warm (cold) PDO phase induces northward (southward) shift of the NEC bifurcation, which enhances (reduces) the KI (Wu, 2013; Wu et al., 2016). The weakening trend of the KI, −0.12 Sv/year from 1993 to 2012, estimated from satellite data and hydrographic observations across the strait, is likewise attributed to the changes in PDO phase (Nan et al., 2016). Due to the predominantly cold (negative) PDO regime since the early 1990s, the position of the NEC bifurcation latitude is southward, lessening the penetration of the KI into the SCS (Nan et al., 2016; Wu, 2013). Another study highlights the role of long-term changes in pressure gradient on the reduction of KI across the strait in the recent decades (e.g., Nan et al., 2013). Whether the intrusion is linked with the ENSO or PDO and driven by the local and large-scale wind forcing or pressure difference across the strait still remains a subject of disagreement (Nan et al., 2015).

Paleoreconstructions based on both marine sediments and coral proxies provide insights into the long-term change of Kuroshio transport. Changes in planktonic foraminiferal assemblages and stable isotope geochemistry reveal fluctuations in Kuroshio flow patterns and intensities along the east coast of Japan since the Late Quaternary to the Holocene (e.g., Jian et al., 2000; Ujiie & Ujiie, 1999). Similarly, coral $\delta^{15}N$ and $\delta^{18}O$ from east of Japan and south of Taiwan record Kuroshio variability in the last 50 to ~150 years (e.g., Li et al., 2017; Yamazaki et al., 2016). Paleoreconstruction of the KI strength, on the other hand, is limited to the Holocene (e.g., Liu et al., 2013), where ENSO-related mechanisms remained unclear. While direct measurements, satellite data, numerical models, and proxy reconstructions have advanced our present-day knowledge of current movements and transport variability in recent decades, there is still a need for multidecadal, high-resolution on-site LST records to better understand its interannual variation.

This study presents annually resolved histories of mean transport variability across the LS based on coral radiocarbon ($\Delta^{14}C$) records. In this approach, we aim to investigate how the surface transport across the LS has changed in the past 68 years. Moreover, we aim to provide insights on the possible mechanisms that drive its variability. This information is critical to understanding the causes and impacts of long-term ocean circulation variability in this region.

1.1. Radiocarbon as a Tracer of Ocean Circulation

Radiocarbon (^{14}C) is naturally produced in the upper atmosphere through the collision of cosmic ray neutrons and ^{14}N (Anderson et al., 1947; Broecker, 2014). The resultant ^{14}C rapidly oxidizes to $^{14}CO_2$ gas and is distributed in the Earth's carbon reservoirs. In the surface ocean, atmospheric ^{14}C is admitted into seawater and becomes part of the dissolved inorganic carbon (DIC) pool with a $\Delta^{14}C_{DICsw}$ that is lower than that in the atmosphere. Relative to the surface, deeper waters have lower $\Delta^{14}C$ values because of isolation from the atmosphere and subsequent radioactive decay. Consequently, upwelling or vertical mixing introduces older and deeper water to the surface resulting in an overall lowering of $\Delta^{14}C_{DICsw}$ values. During the late 1950s and early 1960s, thermonuclear bomb testing increased the difference between the surface

and deep ocean $\Delta^{14}C$ values, making ^{14}C a more sensitive tracer of ocean circulation and mixing (Broecker, 2014; Grottoli & Eakin, 2007).

Corals utilize calcium and DIC in seawater for the production of aragonite ($CaCO_3$), hence changes in the $\Delta^{14}C_{DICsw}$ through time are stored in the $CaCO_3$ skeleton of the corals (Druffel, 1997a; Grottoli & Eakin, 2007). Relative to other coral proxy records, $\Delta^{14}C_{coral}$ is not affected by biological process; thus, they provide a conservative tracer of ocean circulation (Dunbar & Cole, 1999). Coral $\Delta^{14}C$ records of various temporal resolution and length are available in the WPO, SCS and Indonesia regions (Figure 1). These records provide histories of basin-scale changes in ocean circulation since the beginning of the twentieth century. In conjunction with our coral $\Delta^{14}C$ records, we take advantage of this extensive spatial and temporal information to examine the interaction between the WPO and the SCS through the LS.

2. Coral Sampling and Analytical Methods

2.1. Coral Sites and Sampling

In May 2013 and May 2012, vertical cores of *Porites* sp. were drilled underwater in Houbihu, Nanwan Bay, Taiwan (21.9°N, 120.7°E), and offshore Palaui Island, Philippines (18.5°N, 122.2°E), at 4- to 6-m depths, respectively (Figure 1). The ~3-m and 2-m-long cores from Houbihu and Palaui, respectively, were cut, slabbed, and X-radiographed to reveal annual density banding. Select years between 1942 and 2010 identified using annual density bands and high-resolution Sr/Ca time series (e.g., Ramos et al., 2017) were subsampled using a tungsten carbide drill burr attached in a Dremel® tool. Select years from 1952 to 2010 were additionally scored parallel to the growth bands at subannual resolution (approximately four to six samples per year, width of 2 to 3 mm) to further examine the seasonal $\Delta^{14}C$ variability at each site. Age errors are estimated to be roughly 1 to 2 months based on comparing the seasonal $\Delta^{14}C$ record and seasonally averaged Sr/Ca data.

2.2. $\Delta^{14}C$ Measurements

Seven to 8-mg aragonite powder samples were acidified with 85% phosphoric acid to produce CO_2 gas. The resultant CO_2 gas was subsequently purified and converted to graphite on Fe powder using the Zn reduction method (Xu et al., 2007). The graphite was then analyzed for ^{14}C using an accelerator mass spectrometer at the Keck Carbon Cycle accelerator mass spectrometer laboratory using standard techniques (Southon et al., 2004). Backgrounds were subtracted using measurements of ^{14}C-free, spar calcite. The ^{14}C measurements are reported as Δ values that are corrected for known age to 1950 (Stuiver & Polach, 1977). Analytical precision is ±1.5‰ based on long-term analyses of a modern coral standard (CSTD) and duplicate measurements of samples.

3. Results

3.1. LS $\Delta^{14}C$ Record

Seventy-nine annual and 228 seasonal $\Delta^{14}C$ samples from the Houbihu and Palaui coral cores were analyzed covering the last 68 years (Figure 2a and Data Set S1 in the supporting information). From the prebomb period of 1942 to 1953, Houbihu coral $\Delta^{14}C$ values ranged from −68.0‰ to −60.9‰ and were lower than those from Palaui, which ranged from −60.6‰ to −56.2‰. Early bomb-produced ^{14}C spikes are recorded in both corals in 1955, increasing by 45.0‰ and 69.4‰ from the Houbihu and Palaui prebomb values, respectively. Both $\Delta^{14}C$ values decreased slightly in 1956 to 1957 and began to increase rapidly following the input of more bomb ^{14}C. Bomb tests during this period obscured seasonality in both $\Delta^{14}C$ records.

The highest $\Delta^{14}C$ values were recorded in the early 1970s, approximately 10 years after the atmospheric bomb peak (Nydal, 2000, Figure 2a), reaching a maximum of 149.7‰ in Houbihu and 165.2‰ in Palaui. Subsequently, the bomb curves decreased at a rate of about ~3‰/year. The seasonality in the records became more distinct during this period, where Palaui shows greater variability than Houbihu especially in the early 1970s (F test, two tailed, $p = 0.0008$, Figure 2a). Compared to the mean surface zonal current direction across the strait derived from Simple Ocean Data Assimilation data set (SODA v.2.2.4, Carton & Giese, 2008, see details in Figure 1), Houbihu seasonal $\Delta^{14}C$ maxima (minima) coincided with westward (eastward) current flows (Figure 3). The short and discontinuous seasonal $\Delta^{14}C$ records prevent us from statistically quantifying

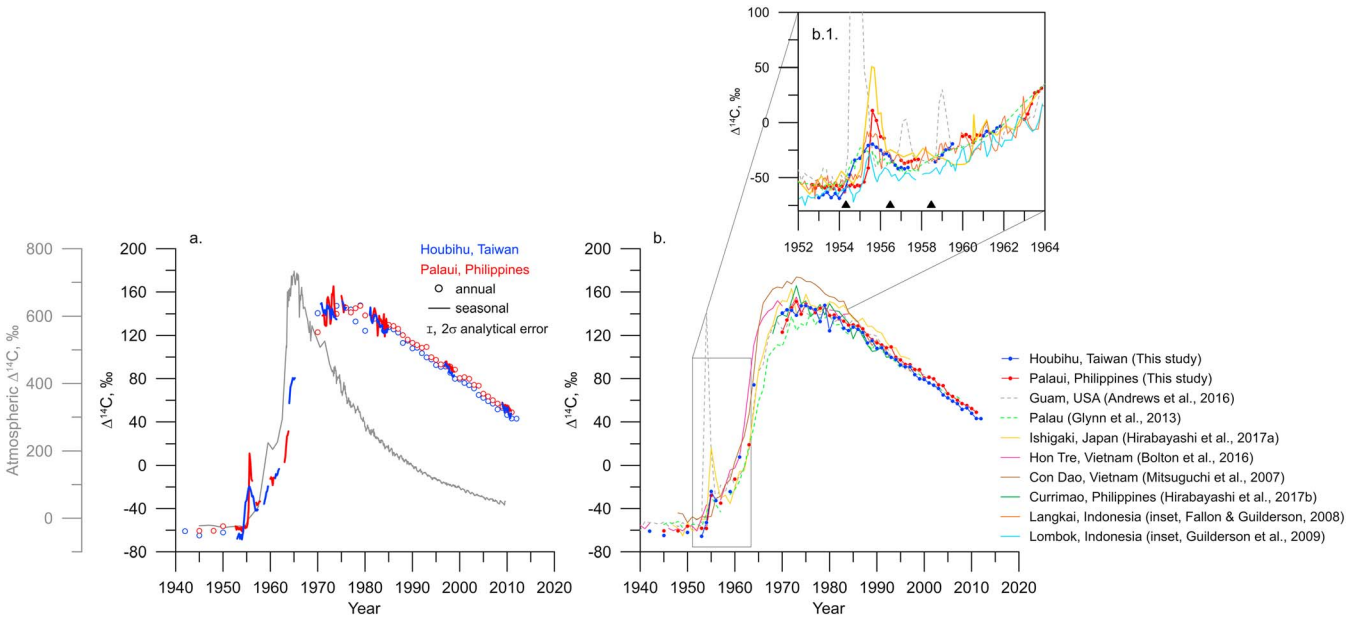

Figure 2. (a) Annual (open circles) and seasonal (solid lines) coral $\Delta^{14}C$ from Houbihu (blue) and Palaui (red) from 1942 to 2011. (b) Annual $\Delta^{14}C$ records from this study compared to Western Pacific Ocean, South China Sea, and Indonesian Throughflow records. (See also Figure S1 in the supporting information.) Inset (b.1) shows the early bomb records from these sites. Black triangles indicate the timing of the bomb-testing operations in the Pacific (Andrews et al., 2016).

this relationship at this site. However, considering that the surface flow across the LS is far more complex than presented here, the observed general agreement between records provides indication that zonal flow influences Houbihu $\Delta^{14}C$ seasonality. In contrast, the timing of the Palaui seasonal $\Delta^{14}C$ maxima and minima was more variable with respect to the mean flow direction (Figure 3). In addition, the Palaui $\Delta^{14}C$ record was on average ~4‰ higher than the Houbihu record, which is greater than the propagated

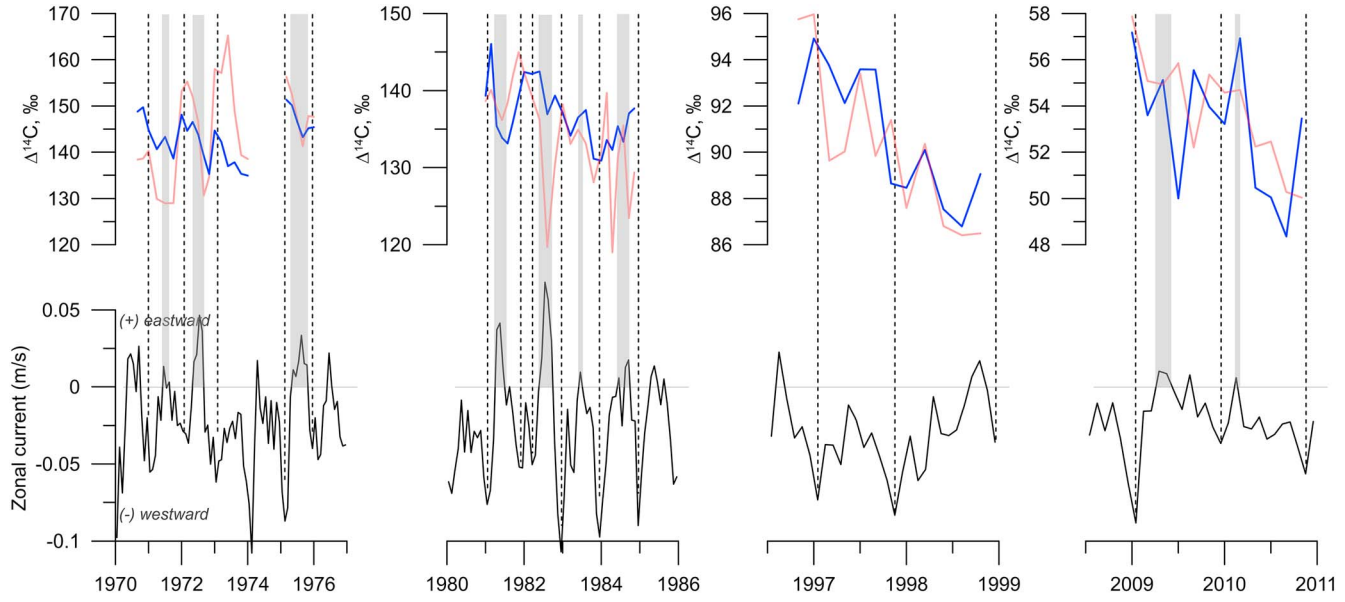

Figure 3. Houbihu (blue) and Palaui (red) seasonal $\Delta^{14}C$ record compared with surface zonal currents averaged along 120.8°N (see Figure 1). Dashed lines (shaded areas) represent the northeast (southwest) monsoon season where the general current direction is westward (eastward). In general, Houbihu $\Delta^{14}C$ seasonal maxima (minima) coincides during the northeast (southwest) monsoon seasons. Palaui $\Delta^{14}C$ maxima and minima, on the other hand, show variable timing with respect to the mean flow direction.

analytical error of 2.1‰ (Figure 2a) suggesting that Palaui and Houbihu are influenced by different water masses and/or surface processes.

3.2. Regional $\Delta^{14}C$ Variability

Compared with the WPO and SCS annual records (Figure 1), Houbihu prebomb $\Delta^{14}C$ values are lower than most other records in the region (i.e., -64.6 ± 2.5‰, $n = 8$, 1σ, Figure 2b). In contrast, Palaui prebomb $\Delta^{14}C$ (-58.4 ± 1.6‰, $n = 12$, 1σ) is regionally comparable to Hon Tre, Vietnam (-57.1 ± 3.7‰, $n = 10$, 1σ, Bolton et al., 2016), Ishigaki, Japan (-57.9 ± 7.6‰, $n = 18$, 1σ, Hirabayashi, Yokoyama, Suzuki, Miyairi, & Aze, 2017), Guam (-54.0 ± 5.4‰, $n = 18$, 1σ, Andrews et al., 2016), and Palau (-54.9 ± 2.4‰, $n = 9$, 1σ, Glynn et al., 2013; Figure 2b). Con Dao, Vietnam (-47.9 ± 3.3‰, $n = 6$, 1σ, Mitsuguchi et al., 2007) on the SCS shelf has the highest $\Delta^{14}C$ values during this period (Figure 2b).

Initial $\Delta^{14}C$ bomb spikes in 1954 and 1955 are not evident in the SCS records but are distinct in the WPO, Indonesian Throughflow (ITF) records (i.e., Langkai, Fallon & Guilderson, 2008, and Lombok, Guilderson et al., 2009, Indonesia, Figure 2b.1), and our sites, indicating the role of the location and distance between sites in the delivery of bomb-contaminated waters and its preservation in the coral skeletons. The early $\Delta^{14}C$ spikes were attributed to the early thermonuclear tests conducted in Bikini and Enewatak Atolls in the Pacific in 1954. Guam, nearest to the atolls, shows the earliest $\Delta^{14}C$ increase (i.e., ~3 months after the initial test) and the most pronounced spike (i.e., ~710‰ in the seasonal record, not shown, Andrews et al., 2016). Guam also shows distinct bomb-related peaks in 1957 and 1959, similarly captured by the high-resolution $\Delta^{14}C$ record in Ishigaki, but with a year lagged (Andrews et al., 2016; Hirabayashi, Yokoyama, Suzuki, Miyairi, & Aze, 2017). Palau, nearest to Guam, records an early $\Delta^{14}C$ rise in 1954 but sustained a lower bomb peak that lasted until late 1956 (Glynn et al., 2013). Houbihu $\Delta^{14}C$ shows an earlier rise and broader bomb peak than that of Palaui, but both records reached initial peak values in mid-1955, a year after the early bomb detonations. Langkai and Lombok $\Delta^{14}C$ records show the same initial rise in mid-1955 (Fallon & Guilderson, 2008; Guilderson et al., 2009), within the same time period as our sites (±1 to 2 months), which may highlight the similar transport times between the bomb-contaminated waters—the Pacific western boundary currents (i.e., NEC, KC, and MC) and the ITF and between the Pacific western boundary current and the KI. Moreover, the smaller $\Delta^{14}C$ peaks and the absence of other bomb-related peaks in the late 1950s in the ITF and our records suggest other water mass exchanges along these passageways.

In the 1960s, Houbihu $\Delta^{14}C$ along with other SCS records rose earlier than those of Palaui and the WPO (Figure 2b). In the following decade, all records reached the postbomb $\Delta^{14}C$ peak showing variable amplitude and timing of the peak. WPO records reached the postbomb peak in 1972. Ishigaki records the highest $\Delta^{14}C$ peak (i.e., 163.1‰), while Guam and Palau recorded 150‰ and 137.8‰, respectively. The SCS records, on the other hand, peaked in 1973 and recorded higher postbomb values than the WPO. Con Dao and Currimao, Philippines, (Hirabayashi, Yokoyama, Suzuki, Miyairi, Aze, Siringan, & Maeda, 2017) recorded the highest values at 173.8‰ and 165.8‰, respectively, while Hon Tre recorded 155.3‰. Palaui (151.2‰) and Houbihu (147.2 ‰) $\Delta^{14}C$ values are comparable to Guam.

In the postbomb period after the 1970s (Figure 2b), when lateral advection and vertical mixing mainly controls the surface ocean $\Delta^{14}C$ variability, Palaui shows more variability compared to Guam that, except for the post bomb peak and early 1980s, exhibits a 16-year plateau that lasted until 1986 (Andrews et al., 2016). Houbihu $\Delta^{14}C$ values are close to Palaui in the early 1970s and subsequently fluctuated between those of Currimao and Guam in the mid-1980s. Ishigaki and Con Dao $\Delta^{14}C$ values remained higher than the other records. Con Dao and Hon Tre values approach the WPO records in the mid-1980s. The $\Delta^{14}C$ differences between sites and its potential drivers will be further investigated in the following section.

4. Discussion

Compared with Houbihu, higher $\Delta^{14}C$ values in Palaui may reflect the constant influence of water masses with a greater exposure to the atmosphere. Gyre and gyre-fed western boundary currents, like the Kuroshio that passes east of Luzon, have generally long residence times at the surface (Grottoli & Eakin, 2007; Mahadevan, 2001). This enables air-sea CO_2 exchange to increase $\Delta^{14}C$, as long as $\Delta^{14}C$ in the air remains higher than that in the surface water. The lower $\Delta^{14}C$ values in Houbihu, on the

other hand, suggest regular renewal of surface waters from those at depth that contain lower $\Delta^{14}C$ values. Tidally induced upwelling from the depths of 100 to 200 m offshore occurs in Houbihu on a daily basis (Lee, Chao, & Fan, 1999; Lee, Chao, Fan, & Kuo, 1999; Lee et al., 1997), likely causing the dilution of surface $\Delta^{14}C$ with lower $\Delta^{14}C$ values and the observed dampening in $\Delta^{14}C$ seasonality at this site. However, since the LS is a site of water mass exchange between the SCS and the WPO, the $\Delta^{14}C$ values at our sites must be additionally affected by the $\Delta^{14}C$ variability between these basins.

The occurrence of early bomb peaks in both Houbihu and Palaui $\Delta^{14}C$ records indicates influence of the western Pacific circulation across the LS. Relative to air-sea CO_2 exchange, which typically takes a decade (Nydal, 2000), the quick $\Delta^{14}C$ rise in Houbihu and Palaui recorded 1 year after the initial bomb detonations is likely due to a nuclear fallout signal distributed by the advection of tropical Pacific currents (i.e., NEC and KC) originating at the testing sites at Bikini and Enewetak atolls (Andrews et al., 2016; Glynn et al., 2013; Hirabayashi, Yokoyama, Suzuki, Miyairi, & Aze, 2017). This current system delivers bomb-contaminated NEC waters through Guam, with a current speed of ~0.1 to 0.2 m/s, until it bifurcates to the northward flowing KC and the southward flowing MC whose speeds are roughly 5 to 10 times faster (Andrews et al., 2016; Lien et al., 2014; Qu et al., 1998; Figure 1). The difference in the transport velocities between the NEC and its branches (i.e., KC and MC) explains the 1-year lag time between the initial detonations and the early bomb peaks in the coral records (Hirabayashi, Yokoyama, Suzuki, Miyairi, & Aze, 2017).

In the Pacific, the interannual variability of the location and speed of the western boundary currents are strongly influenced by ENSO (Y. Y. Kim et al., 2004; Qiu & Chen, 2010). To further investigate this control on the $\Delta^{14}C$ variability at our sites during the post bomb period (i.e., after 1970), we compared our results with Guam $\Delta^{14}C$ since the Kuroshio waters reaching our sites originate from the NEC that flow by Guam. Compared to other WPO sites, Palau, located south of the NEC (i.e., in the North Equatorial Counter Current) experiences vertical mixing induced by the MC-North Equatorial Counter Current interaction (Glynn et al., 2013). Offshore Ishigaki is influenced by eddy activities dominating the downstream end of the Kuroshio (Hirabayashi, Yokoyama, Suzuki, Miyairi, & Aze, 2017), far beyond the LS. We found that the interannual $\Delta^{14}C$ difference between Palaui and Guam is statistically correlated with the meridional shift of the NEC bifurcation latitude (NBL hereafter; e.g., Qiu & Chen, 2010) with a 1-year lag ($r = 0.65$, $p = 0.001$, $n = 21$, Figure 4a) from 1980 to 2000. Positive (negative) Palaui-Guam $\Delta^{14}C$ difference corresponds to the northerly (southerly) position of the NBL. Wind-induced NBL migration and the offshore Kuroshio transport velocities are well correlated with ENSO (e.g., Niño 3.4—Qiu & Chen, 2010, Figure 3a); and the Southern Oscillation Index (Y. Y. Kim et al., 2004). During El Niño years, the northward NBL position causes less NEC water to flow northward to the KC relative to the southward flow east of Mindanao (Y. Y. Kim et al., 2004; Qiu & Chen, 2010; Qiu & Lukas, 1996). Due to the dampened winds, the NEC and Kuroshio velocities are slower, and transports are at their minimum during El Niño (Y. Y. Kim et al., 2004; Qiu & Chen, 2010; Qiu & Lukas, 1996). This leads to a positive Palaui-Guam $\Delta^{14}C$ difference (i.e., Palaui $\geq$ Guam) where the slow-moving currents induce more surface $\Delta^{14}C_{DICsw}$ entrainment. Conversely, La Niña years are associated with the southward NBL migration, faster and greater NEC and Kuroshio transports leading to less surface water entrainment and, therefore, higher $\Delta^{14}C$ values in Guam than Palaui. The observed NBL anomaly leading the Palaui-Guam $\Delta^{14}C$ difference by a year may be explained by the difference in transport velocities between the NEC and Kuroshio as previously discussed above.

Prior to 1980, the positive Palaui-Guam $\Delta^{14}C$ difference during 1970–1971, 1975–1976, and 1979 is opposite of what the above mechanism predicts. This period coincides with the broad $\Delta^{14}C$ plateau recorded in Guam (Andrews et al., 2016). The cause of the small $\Delta^{14}C$ variability after the bomb peak in Guam is not well understood (Andrews et al., 2016). However, the higher $\Delta^{14}C$ values in Palaui and other sites at the downstream end of KC (i.e., Houbihu and Ishigaki) and the SCS compared to Guam may indicate a forcing not related to the position of the NEC latitude and/or ENSO. We further investigate by similarly taking the $\Delta^{14}C$ difference between Ishigaki and Guam. The variability in Ishigaki-Guam $\Delta^{14}C$ difference is likewise controlled by the bifurcation latitude after 1980 and not before this period ($r = 0.54$, $p = 0.02$, $n = 18$). We hypothesize that the postbomb peak in 1973 has obscured the NBL-related surface water entrainment, where the higher and spatially variable $\Delta^{14}C$ distribution at these sites during this period precedes the mean circulation patterns. Other possible mechanisms include the influence of local oceanographic processes such

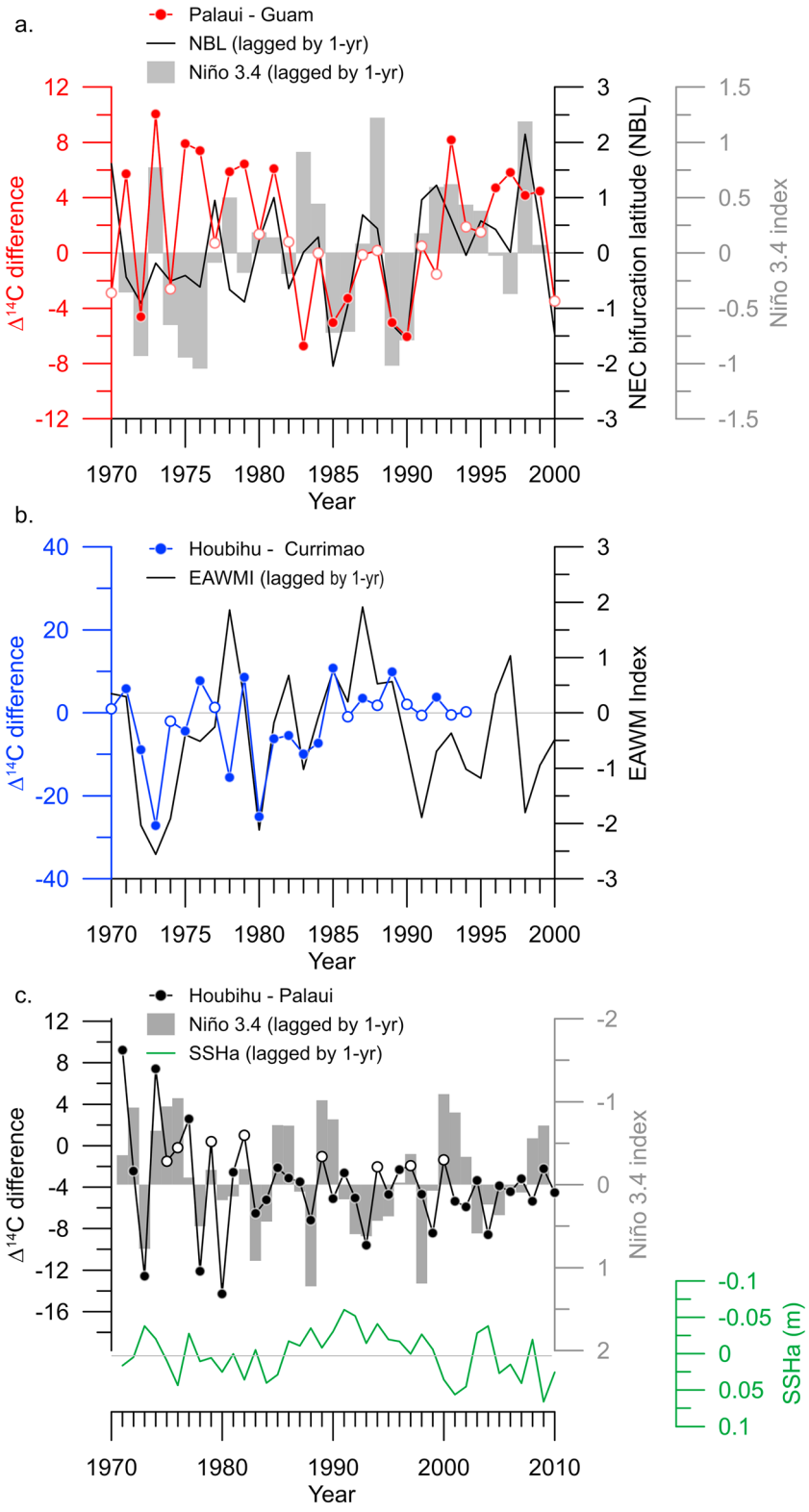

Figure 4. $\Delta^{14}C$ difference between (a) Palaui and Guam compared with the NEC bifurcation latitude (Qiu & Chen, 2010) and the Niño 3.4 index, (b) Houbihu and Currimao compared with the EAWM index (D'Arrigo et al., 2005), and (c) Houbihu and Palaui compared with the Niño 3.4 index (gray bars, reversed axis) and Simple Ocean Data Assimilation-derived sea surface height anomalies (green SSHa). Hollow dots indicate that the $\Delta^{14}C$ difference between records is 0 (i.e., the $\Delta^{14}C$ values being compared are statistically equivalent). NEC = North Equatorial Current; NBL = NEC bifurcation latitude; EAWMI = East Asian Winter Monsoon index.

as occurrence of mesoscale eddies and upwelling (e.g., Ishigaki, Hirabayashi, Yokoyama, Suzuki, Miyairi, Aze, Siringan, & Maeda, 2017). In contrast with the Palaui-Guam $\Delta^{14}C$ difference, Houbihu-Guam $\Delta^{14}C$ is not correlated with the NBL migration ($r = 0.22$, $p = 0.24$, $n = 31$, not shown), likely due to its inward location within the strait where offshore Kuroshio influence is driven by the KI.

Relative to the seasonal $\Delta^{14}C$ records in the WPO including Palaui (not shown), the seasonality in Houbihu $\Delta^{14}C$ is more regular. Seasonal highs and lows generally follow the timing of the westward and eastward flow directions across the strait. (See section 3.1 and Figure 3.) This may indicate that the controlling factor in the alternating flow patterns across the strait may be preserved in the Houbihu $\Delta^{14}C$ record. Both the mean surface flow across the strait and surface circulation in the SCS are strongly dependent on the Asian monsoon system (e.g., Centurioni et al., 2004; G. Chen, Hu, et al., 2011; Hsin et al., 2012; Metzger & Hurlburt, 1996; Nan et al., 2015; Qu et al., 2004, 2000; Tian et al., 2006; P.-X. Wang & Li, 2009; Wyrtki, 1961; Yang et al., 2010; Yaremchuk & Qu, 2004). During winter, the prevailing northeast monsoon winds drive surface water flow westward across the strait. The general surface circulation within the SCS is also cyclonic during this period (Figure 1). During summer, the general surface circulation involves a cyclonic and anticyclonic circulation in the northern and southern SCS region, respectively (Figure 1).

Between the winter and summer monsoon systems, the East Asian Winter Monsoon (EAWM) has a greater impact on the westward flow across the strait and circulation within the SCS (Hsin et al., 2012). To examine the monsoonal control on the circulation and $\Delta^{14}C$ variability between our sites and the SCS records, we similarly calculated the interannual $\Delta^{14}C$ difference between Houbihu $\Delta^{14}C$ and Con Dao, Hon Tre, and Currimao. Con Dao sits on a continental shelf in shallow waters and is mainly impacted by atmospheric $\Delta^{14}C$ processes (Mitsuguchi et al., 2007). In contrast, Hon Tre and Currimao are monsoon-driven sites with seasonal upwelling and advection impacting $\Delta^{14}C$. Southeast monsoon winds blow parallel to the Vietnam coast at Hon Tre driving summer upwelling at this site (Bolton et al., 2016). $\Delta^{14}C$ in Currimao shows significant correspondence with the strength of the winter monsoon winds (Hirabayashi, Yokoyama, Suzuki, Miyairi, Aze, Siringan, & Maeda, 2017), which drives upwelling and $\Delta^{14}C$ variability along the northwest coast of Luzon (Shaw et al., 1996). Due to these site attributes, only the $\Delta^{14}C$ difference between Houbihu and Currimao shows a significant relationship with the EAWM winds (e.g., D'Arrigo et al., 2005) with a 1-year lag ($r = 0.46$, $p = 0.02$, $n = 25$, Figure 4b). Because of westward intrusions across the strait and upwelling offshore of Currimao during stronger (positive) EAWM periods, the $\Delta^{14}C$ difference between Houbihu and Currimao is positive (i.e., Houbihu > Currimao). Conversely, the SCS outflow is more evident during weak EAWM periods, leading to a negative Houbihu-Currimao $\Delta^{14}C$ difference (i.e., Houbihu < Currimao). The slower currents within the strait and in the northern SCS region (i.e., maximum of 0.35 m/s; J. Hu et al., 2000; Nan et al., 2015) compared with the surrounding waters may explain the 1-year delay.

Across the strait, the interannual $\Delta^{14}C$ difference between Houbihu and Palaui is significantly correlated with ENSO (e.g., Niño 3.4) with a 1-year lag ($r = -0.46$, $p = 0.003$, $n = 41$, Figure 4c). The negative correlation indicates that large (small) $\Delta^{14}C$ differences (i.e., greater/lesser than ~4‰) coincide with El Niño (La Niña) years. The influence of ENSO to the $\Delta^{14}C$ difference between our sites may lie on the meridional pressure difference across the strait. SODA-derived sea surface height (SSH) anomalies, an indicator of pressure difference (See details in Figures 1 and S2.), show a significant negative correlation with ENSO from 1970 to 2010 ($r = -0.48$, $p = 0.007$, $n = 31$, Figure 4c). The negative relationship indicates that El Niño (La Niña) years coincide with lower (higher) SSH anomalies. Since the mean SSH in the western Pacific is higher than that of the SCS (Figure 1), a higher SSH across our sites must be due to the piling-up of water across the strait. During La Niña, the enhanced trade winds push more water toward the western Pacific, leading to higher SSHs in this region, indicating presence of the KI along the strait (Nan et al., 2013, 2015) and, thus, smaller $\Delta^{14}C$ differences between our Houbihu and Palaui sites. Conversely, due to the relaxed trade winds during El Niño, the western Pacific warm pool spreads toward the east, flattening the SSH in this region and increasing the $\Delta^{14}C$ difference between our sites. Other satellite altimetry studies along the strait have shown that SSH anomalies in conjunction with density stratification data are indicative of the presence or absence of the KI along the strait (e.g., DeCarlo et al., 2015). However, whether the KI penetrates into the SCS based on the above $\Delta^{14}C$ differences remains ambiguous.

Overall, basin-specific processes controlling the $\Delta^{14}C$ variability of the LS sites are evident from quantifying the $\Delta^{14}C$ difference between our sites and other $\Delta^{14}C$ records in the region. Palaui $\Delta^{14}C$, relative to that of

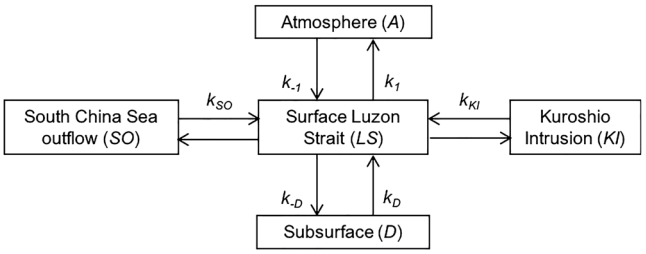

Figure 5. Schematic of the box model used to estimate the lateral advection between the South China Sea and the Pacific. The $\Delta^{14}C$ of the surface box of the Luzon Strait *(LS)* is affected by the inputs from the atmosphere (*A*), the subsurface (*D*) and the lateral contributions from the South China Sea outflow (*SO*) and the Kuroshio Intrusion (*KI*).

Guam, documents the impact of the ENSO-modulated NBL migration in the Pacific on the Kuroshio transport east of Luzon. During El Niño, the Kuroshio influence at Palaui is enhanced. Houbihu $\Delta^{14}C$, relative to that of Currimao, records evidence of the EAWM-driven water mass exchange along the strait and in the northern SCS. A weaker EAWM relatively increases the SCS outflow contribution across the strait. In between our sites, La Niña-related high-pressure gradient across the strait may indicate the occurrence of KI but whether it reaches the SCS remains to be further investigated.

4.1. Box Model Calculation

To integrate the above observations and fully assess the drivers of water transport across the strait, we employed a five-box model based on previous models developed for the North Atlantic and Indian Oceans (Druffel, 1989, 1997b; Goodkin et al., 2012; Grumet et al., 2004). Figure 5 shows the schematic of the box model, which includes the atmosphere (*A*), surface boxes of the LS, KI which implicitly includes the influence of the KC, and SCS outflow (*LS*, *KI*, and *SO*) and the subsurface box of the thermocline (*D*). The inputs and data sources for each box are summarized in Table S1 in the supporting information. Pertinent calculations can also be found in a separate Microsoft Excel® spreadsheet (Table S2) in the supporting information.

With equal amounts lost in the *LS* box to conserve mass, the rate of change in the surface *LS* $\Delta^{14}C$, $\frac{dLS}{dt}$, is affected by air-sea gas exchange *A*, vertical contribution from *D* and lateral advection with inputs from both the *SO* and the *KI*, such that

$$\frac{dLS}{dt} = k_{-1}\left(\frac{A}{0.983} - LS\right) + k_D\,(D - LS) + k_{SO}\,(SO - LS) + k_{KI}\,(KI - LS), \quad (1)$$

where 0.983 is the isotopic fractionation factor describing the influx of CO_2 from the atmosphere to the sea surface (Broecker & Peng, 1982). Box *A* is represented by the annual $\Delta^{14}C$ values of tree ring and atmospheric CO_2 $\Delta^{14}C$ data. The prebomb (1942 to 1953) values are from Stuiver and Quay (1981) and the postbomb (1970 to 2012) values are from Hua et al. (2013). The surface boxes of *LS* and *KI* are represented by the $\Delta^{14}C$ values of corals from our study sites, Houbihu and Palaui, respectively. The values for the surface box *SO* are averaged $\Delta^{14}C$ records from Hon Tre (Bolton et al., 2016), Con Dao (Mitsuguchi et al., 2007), and Currimao (Hirabayashi, Yokoyama, Suzuki, Miyairi, Aze, Siringan, & Maeda, 2017), duly representing the SCS $\Delta^{14}C$ variability in the model. Unlike the other boxes, the subsurface data for *D* are temporally and spatially sparse with no direct measurements across the strait. Box *D* is assumed to have prebomb values (e.g., Ostlund & Stuiver, 1980; Stuiver et al., 1981) between depths of 50 and 200 m, well within the mean penetration depth of bomb ^{14}C (e.g., Peng et al., 1998). The prebomb $\Delta^{14}C$ depth profiles cover a wide area in the North Pacific, between 10–50°N and are estimated from surveys conducted by the Geochemical Ocean Section (GEOSECS) Program in 1973. The postbomb values for *D*, on the other hand, are derived from the succeeding international surveys of the World Ocean Circulation Experiment in 1993 and the Climate and Ocean—Variability, Predictability and Change (CLIVAR) in 2004 and 2006, which are verified and synthesized by the Global Ocean Data Analysis Project (https://cdiac3.ornl.gov/waves/glodapv2/, Lauvset et al., 2016; Olsen et al., 2016). These surveys include transects covering the Northern Pacific gyre but only the westernmost transects (i.e., 15–35°N and 125–145°N) along the path of the Kuroshio are selected (Figure S3). The data in between the available years were then linearly interpolated to construct an annual record of $\Delta^{14}C$ for *D*. This data assumption is supported by the advection of subsurface (i.e., 100 to 200 m) tropical waters from the Pacific into the SCS via the LS evidenced in the Hon Tre coral Pb/Ca signals (e.g., M. Chen et al., 2016). The terms k_{-1}, k_{SO}, k_{KI}, and k_D are the exchange rates between the boxes estimated with respect to the volume of the surface and subsurface boxes. The volume of the *LS* and *D* boxes is calculated using lengths delineating *KI* extension, from 123°E inward to 118°E, widths based on the locations of our coral sites, 18°N to 22°N, and depths where both vertical and lateral exchanges occur, ~200 m (J. Hu et al., 2000; Nan et al., 2015; Shen et al., 2005).

The rate of $^{14}CO_2$ input from the air to the sea surface, k_{-1}, is expressed as follows:

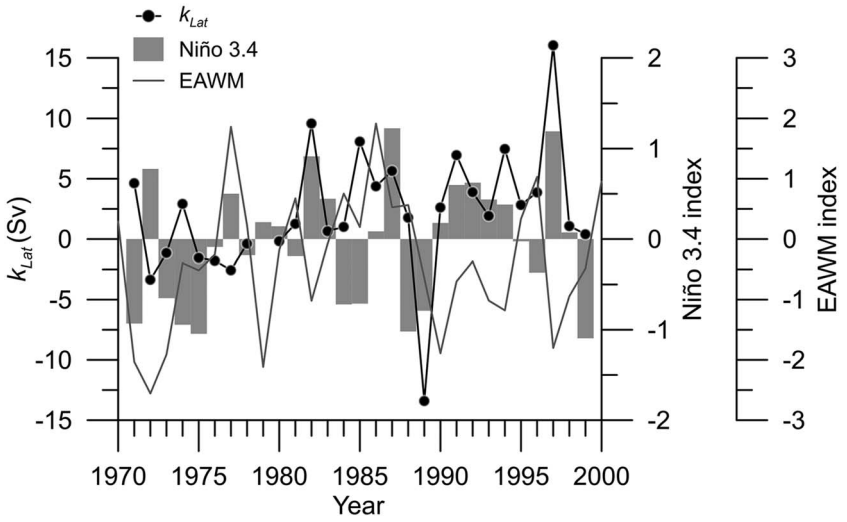

Figure 6. Calculated lateral advection, k_{Lat} (black line with filled circles), compared to the Niño 3.4 (gray bars) and East Asian Winter Monsoon (EAWM) indices (gray line). Positive (negative) values indicate El Niño (La Niña) and strong (weak) EAWM conditions.

$$k_{-1} = \frac{V_p \times \mathrm{CO_2} \times 365\ \mathrm{days/year}}{Z \times \Sigma \mathrm{CO_2}}\ \mathrm{year}^{-1}, \tag{2}$$

where V_p (m/day) is the gas exchange piston velocity, a function of wind speed (WS = 6.4 m/s from National Centers for Environmental Prediction-National Center for Atmospheric Research Reanalysis; Kalnay et al., 1996) and equivalent to V_p = WS * 0.9995–3.47 (Druffel, 1997b; Goodkin et al., 2012; Grumet et al., 2004); $\mathrm{CO_{2(aq)}}$ is the dissolved $\mathrm{CO_2}$ fixed to a value of 0.019 mol/m^3 (Druffel, 1997b; Goodkin et al., 2012; Grumet et al., 2004); Z is the mixed layer depth fixed to a value of 50 m based on the Ocean General Circulation Model for Earth Simulator data set (Masumoto et al., 2004) and National Oceanic and Atmospheric Administration World Ocean Database (Levitus, 1982; Monterey & Levitus, 1997); and $\Sigma\mathrm{CO_2}$ is the total $\mathrm{CO_2}$ dissolved in the surface waters equivalent to 2.06 mol/m^3 (Broecker & Peng, 1982; Levitus, 1982). Thus, k_{-1} is equal to 0.20 year^{-1}.

The exchange rate from the subsurface, k_D, is approximated from the upwelling index reported off southwest Taiwan. The mean upwelling rate is 78.2 m^3/s 100^{-1} m of coastline (i.e., total coastline is ~1,700 km; Ndah et al., 2017). With respect to the volume of the subsurface box (i.e., 3.13×10^{13} m^3), the ventilation rate, k_D, is equivalent to 1.2 year^{-1} or, in terms of the mean amount of water exchanged, about ~1.3 Sv.

To approximate the lateral exchange rates from *SO* and *KI* boxes, we assumed that k_{SO} and k_{KI} are fractions of the total lateral input, k_{Lat}, such that 25% and 75% of k_{SO} and k_{KI} constitutes k_{Lat}, respectively, based on Nan et al. (2015; Table S3). Here, the direction of k_{Lat} represents the mean flow along the strait, which is from the WPO into the SCS. The lateral terms in equation (1) were then expressed in terms of k_{Lat}:

$$\frac{\mathrm{d}LS}{\mathrm{d}t} = k_{-1}\left(\frac{A}{0.983} - LS\right) + k_D\,(D - LS) + k_{\mathrm{Lat}}\,[0.25\,(SO - LS) + 0.75\,(KI - LS)]. \tag{3}$$

Assuming steady state conditions,

$$k_{\mathrm{Lat}} = \frac{-\left[k_{-1}\left(\frac{A}{0.983} - LS\right)\right] - [k_D\,(D - LS)]}{[0.25\,(SO - LS) + 0.75\,(KI - LS)]}, \tag{4}$$

where the average fraction modern (Stuiver & Polach, 1977) values for 1942 to 1953 are A = 0.9770 (−23.0‰); LS = 0.9366 (−63.4‰); KI = 0.9411 (−58.9‰); SO = 0.9456 (−54.4‰); and D = 0.9250 (−75.0‰). In the prebomb steady state conditions, we find that k_{Lat} is equal to 0.37 year^{-1}, where k_{KI} and k_{SO} are 0.28 and 0.09 year^{-1}, respectively. With respect to the volume of the *LS,* the amount of water

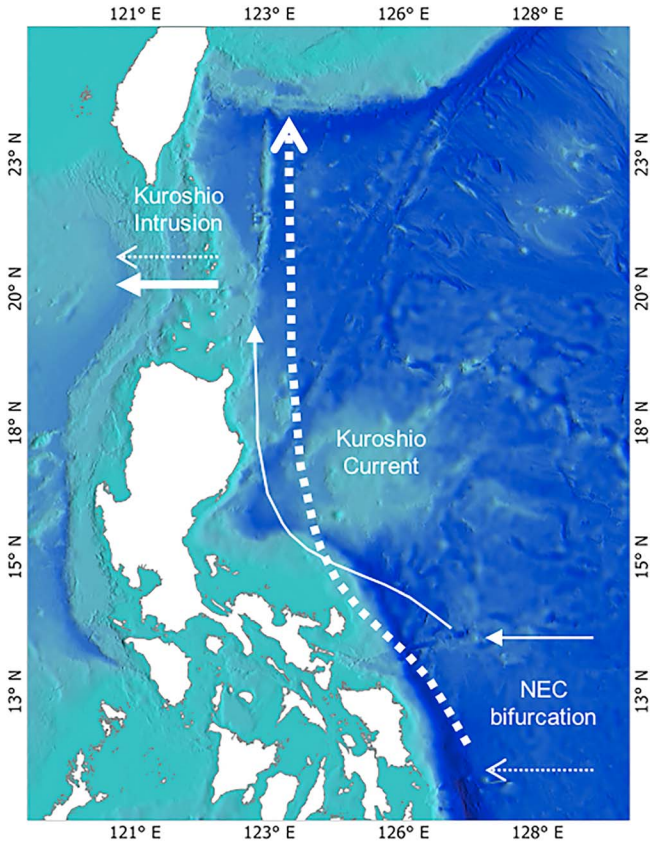

Figure 7. Schematic of the general circulation pattern east of Luzon and across the Luzon Strait during El Niño (solid lines) and La Niña (dashed lines) years. The thickness of the lines and arrows indicate the relative amount of transport. NEC = North Equatorial Current.

exchanged, k_{KI} and k_{SO} are correspondingly equal to 0.11 and 0.04 Sv. Among the calculated exchange rates during the prebomb period, k_D is the highest, highlighting the importance of subsurface ventilation in the Δ^{14}C content of the strait.

We applied this model to the postbomb period after 1970 using constant values for k_{-1} and k_D, and solving for k_{Lat}. We excluded the year 1979 because the values for surface boxes SO, LS, and KI are equivalent (Table S2), resulting in a lateral mass value close to 0 and hence an anomalous estimate of the lateral flux. The mean amount of water exchange from 1970 to 1999 across the strait is 2.2 ± 5.2 Sv (1σ, $n = 28$), ranging from −13.4 to 16 Sv, where a negative value is net flow out of the SCS and a positive flow is into the SCS (Figure 6). These values are within the magnitude of the mean flow measurements across the strait commonly conducted in shorter time periods (e.g., Nan et al., 2015) but are likely to be overestimated due to limitations of the model. While k_D is likely to vary with time, we do not have measurements to inform us of changes to the rate. As the largest flux into the strait, small variability of k_D will have minimal impact on the model. In addition, D Δ^{14}C values are the least constrained through time adding additional uncertainty.

The net lateral exchange rate, k_{Lat}, is significantly correlated with ENSO ($r = 0.42$, $p = 0.03$, $n = 29$, Figure 6), indicating its influence in driving the transport variability across the strait. Higher (lower) k_{Lat} generally coincides with El Niño (La Niña) periods, highlighting ENSO's role in the meridional shifts of the NEC bifurcation latitude and subsequent transport across the LS. During El Niño, the northward position of the NEC bifurcation latitude leads to weaker Kuroshio and stronger intrusion across the strait (Figure 7). The reverse is expected during La Niña conditions. However, in 1971–1972, 1974, 1977, 1984–1985, 1988, and 1996, the k_{Lat} values are on the opposite direction of what the above ENSO relationship predicts. The El Niño years of 1972 and 1977 show a lower k_{Lat} value, while the La Niña years of 1971, 1984–1985, 1988, and 1996 show higher k_{Lat} values. The observed k_{Lat} anomalies at beginning of the record may be impacted by the postbomb peak Δ^{14}C distribution that is not advection related as previously discussed.

Because the EAWM is shown to exert influence on the westward transport across the strait, we also compared these anomalous years with the EAWM index and found that the weaker (stronger) monsoon strength in 1972 (1984–1985, 1988, and 1996) may explain the above discrepancies. Weaker EAWM during an El Niño event may indicate the relative dominance of k_{SO} to k_{KI} in 1972. A stronger EAWM during a La Niña event, on the other hand, may enhance overall k_{Lat} across the strait. However, the negative relationship between ENSO and EAWM is not consistent for each ENSO period such that not all weak (strong) EAWM coincides with El Niño (La Niña) years (e.g., D'Arrigo et al., 2005). The PDO may impact the ENSO-EAWM relationship (e.g., J.-W. Kim et al., 2014; L. Wang et al., 2008) and hence the lateral transport across the strait (e.g., Wu, 2013; Wu et al., 2016). However, we do not find a significant relationship between ENSO and the EAWM at different PDO phases and between k_{Lat} and PDO ($p > 0.10$). Due to the length of the record, the interdecadal modulation of the PDO may not be apparent. Nevertheless, the time-varying response of the EAWM to ENSO, regardless of the PDO phase, gives indication of the secondary control of the reversing monsoons over the lateral advection across the strait.

5. Summary and Conclusions

Interannual histories of the mean transport across the LS based on coral-derived Δ^{14}C records show that Houbihu (Taiwan) Δ^{14}C is lower compared to Palaui (Philippines). Both Houbihu and Palaui Δ^{14}C records show early bomb-produced spikes as a result of a nuclear fallout signal carried by the tropical Pacific western boundary currents. The early Δ^{14}C spikes at our sites and the WPO records indicate that circulation in the

Pacific has direct influence on the strait but does not reach the SCS sites. During the postbomb period, Palaui $\Delta^{14}C$ relative to that of Guam generally shows entrainment of surface waters modified by the ENSO-driven shifts of the NEC bifurcation latitude. This highlights the continued influence of the Pacific circulation patterns on the Palaui $\Delta^{14}C$ record. This signal is absent in the Houbihu $\Delta^{14}C$ record, but when compared to that of Currimao (west side of Luzon), the $\Delta^{14}C$ difference between these sites shows a significant relationship with the EAWM, the main driver of the SCS general circulation and alternating flow patterns across the strait. While the ENSO-driven pressure difference between our sites offers support on the occurrence of KI across the strait, whether KI reaches the SCS remains unclear. In conjunction with other $\Delta^{14}C$ records in the region, we were able to calculate the changes in the lateral transport across the strait. The mean amount of water exchanged across the strait from after the postbomb peak is 2.2 Sv, ranging from −13.4 to 16 Sv, where a positive (negative) value indicates net flow into (out of) the SCS. By shifting the position of the NEC bifurcation latitude, ENSO plays a critical role on the interannual variability of water mass exchange across the LS and circulation and water mass renewal in the SCS.

Acknowledgments
The authors would like to thank K. Hughen and J. Ossolinski for fieldwork. Additional help in the field was also provided by J. Aggangan, J. Quevedo, R. Lloren, G. Albano, J. Perez, and A. Bolton in the Philippines and S. Murty, A. Bolton, L. Tsai, R. Tan, S. Doo, I. Suprihanto, and D. Prayudi in Taiwan. We thank S. Griffin for the $\Delta^{14}C$ analysis. The detailed comments and suggestions of two anonymous reviewers significantly improved the original manuscript. Coral $\Delta^{14}C$ data set and box model calculations are available in the supporting information. This research was funded by the National Research Foundation Singapore under its Singapore NRF Fellowship scheme awarded to N. F. Goodkin (National Research Fellow award NRF-RF2012-03), as administered by the Earth Observatory of Singapore and the Singapore Ministry of Education under the Research Centres of Excellence initiative and by the Ministry of Education, Singapore through its Academic Research Fund Tier 2 (Project MOE2016-T2-1-016). This work is a part of the International Atomic Energy Agency (IAEA) Coordinated Research Project K41015. This work comprises Earth Observatory of Singapore contribution 229.

References

Anderson, E. C., Libby, W. F., Weinhouse, S., Reid, A. F., Kirshenbaum, A. D., & Grosee, A. V. (1947). Radiocarbon from cosmic radiation. *Science*, *105*(2735), 576–577. https://doi.org/10.1126/science.105.2735.576

Andrews, A. H., Asami, R., Iryu, Y., Kobayashi, D. R., & Camacho, F. (2016). Bomb-produced radiocarbon in the western tropical Pacific Ocean: Guam coral reveals operation-specific signals from the Pacific Proving Grounds. *Journal of Geophysical Research: Oceans*, *121*, 6351–6366. https://doi.org/10.1002/2016JC012043

Bolton, A., Goodkin, N. F., Druffel, E. R. M., Griffin, S., & Murty, S. A. (2016). Upwelling of Pacific Intermediate Water in the South China Sea revealed by coral radiocarbon record. *Radiocarbon*, *58*(01), 37–53. https://doi.org/10.1017/RDC.2015.4

Broecker, W. S. (2014). Radiocarbon. In K. Turekian & H. Holland (Eds.), *Treatise on geochemistry* (2nd ed., Vol. 5, pp. 257–271). San Diego, La Jolla, CA: University of California, Elsevier Science.

Broecker, W. S., & Peng, T.-H. (1982). *Tracers in the sea*. Palisades, New York: Lamont-Doherty geological observatory, Columbia University.

Carton, J. A., & Giese, B. S. (2008). A reanalysis of ocean climate using Simple Ocean Data Assimilation (SODA). *Monthly Weather Review*, *136*(8), 2999–3017. https://doi.org/10.1175/2007MWR1978.1

Caruso, M. J., Gawarkiewicz, G. G., & Beardsley, R. C. (2006). Interannual variability of the Kuroshio Intrusion in the South China Sea. *Journal of Oceanography*, *62*(4), 559–575. https://doi.org/10.1007/s10872-006-0076-0

Centurioni, L., Niiler, P., & Lee, D.-K. (2004). Observations of inflow of Philippine sea surface water into the South China Sea through the Luzon Strait. *Journal of Physical Oceanography*, *34*, 113–121.

Chen, C.-T. A., Wang, S.-L., Wang, B.-J., & Pai, S.-C. (2001). Nutrient budgets for the South China Sea basin. *Marine Chemistry*, *75*(4), 281–300. https://doi.org/10.1016/S0304-4203(01)00041-X

Chen, C.-T. A., Yeh, Y.-T., Chen, Y.-C., & Huang, T.-H. (2015). Seasonal and ENSO-related interannual variability of subsurface fronts separating West Philippine Sea waters from South China Sea waters near the Luzon Strait. *Deep Sea Research Part I: Oceanographic Research Papers*, *103*, 13–23. https://doi.org/10.1016/j.dsr.2015.05.002

Chen, G., Hou, Y., & Chu, X. (2011). Water exchange and circulation structure near the Luzon Strait in early summer. *Chinese Journal of Oceanology and Limnology*, *29*(2), 470–481. https://doi.org/10.1007/s00343-011-0198-0

Chen, G., Hu, P., Hou, Y., & Chu, X. (2011). Intrusion of the Kuroshio into the South China Sea, in September 2008. *Journal of Oceanography*, *67*(4), 439–448. https://doi.org/10.1007/s10872-011-0047-y

Chen, M., Goodkin, N. F., Boyle, E. A., Switzer, A. D., & Bolton, A. (2016). Lead in the western South China Sea: Evidence of atmospheric deposition and upwelling. *Geophysical Research Letters*, *43*, 4490–4499. https://doi.org/10.1002/2016GL068697

Chern, C.-S., & Wang, J. (1998). A numerical study of the summertime flow around the Luzon Strait. *Journal of Oceanography*, *54*(1), 53–64. https://doi.org/10.1007/BF02744381

D'Arrigo, R., Wilson, R., Panagiotopoulos, F., & Wu, B. (2005). On the long-term interannual variability of the East Asian winter monsoon. *Geophysical Research Letters*, *32*, L21706. https://doi.org/10.1029/2005GL023235

DeCarlo, T. M., Karnauskas, K. B., Davis, K. A., & Wong, G. T. F. (2015). Climate modulates internal wave activity in the Northern South China Sea. *Geophysical Research Letters*, *42*, 831–838. https://doi.org/10.1002/2014GL062522

Druffel, E. R. M. (1989). Decade time scale variability of ventilation in the North Atlantic: High-precision measurements of bomb radiocarbon in banded corals. *Journal of Geophysical Research*, *94*(C3), 3271. https://doi.org/10.1029/JC094iC03p03271

Druffel, E. R. M. (1997a). Geochemistry of corals: Proxies of past ocean chemistry, ocean circulation, and climate. *Proceedings of the National Academy of Sciences*, *94*(16), 8354–8361. https://doi.org/10.1073/pnas.94.16.8354

Druffel, E. R. M. (1997b). Pulses of rapid ventilation in the North Atlantic surface ocean during the past century. *Science*, *275*(5305), 1454–1457. https://doi.org/10.1126/science.275.5305.1454

Du, C., Liu, Z., Dai, M., Kao, S. J., Cao, Z., Zhang, Y., Huang, T., et al. (2013). Impact of the Kuroshio intrusion on the nutrient inventory in the upper northern South China Sea: Insights from an isopycnal mixing model. *Biogeosciences*, *10*(10), 6419–6432. https://doi.org/10.5194/bg-10-6419-2013

Dunbar, R. B., & Cole, J. E. (1999). Annual Records of Tropical Systems (ARTS). In, *PAGES Workshop Report, Series 99–1* (pp. 72).

Fallon, S. J., & Guilderson, T. P. (2008). Surface water processes in the Indonesian throughflow as documented by a high-resolution coral $\Delta^{14}C$ record. *Journal of Geophysical Research*, *113*, C09001. https://doi.org/10.1029/2008JC004722

Glynn, D., Druffel, E. R. M., Griffin, S., Dunbar, R., Osborne, M., & Sanchez-Cabeza, J. A. (2013). Early bomb radiocarbon detected in Palau archipelago corals. *Radiocarbon*, *55*(03), 1659–1664. https://doi.org/10.1017/S0033822200048578

Goodkin, N. F., Druffel, E. R. M., Hughen, K. A., & Doney, S. C. (2012). Two centuries of limited variability in subtropical North Atlantic thermocline ventilation. *Nature Communications*, *3*(1. https://www.ncbi.nlm.nih.gov/pubmed/22549832). https://doi.org/10.1038/ncomms1811

Gordon, A. L., Flament, P., Villanoy, C. L., & Centurioni, L. (2014). The nascent Kuroshio of Lamon Bay. *Journal of Geophysical Research: Oceans*, *119*, 4251–4263. https://doi.org/10.1002/2014JC009882

Gordon, A. L., Huber, B. A., Metzger, E. J., Susanto, R. D., Hurlburt, H. E., & Adi, T. R. (2012). South China Sea throughflow impact on the Indonesian throughflow. *Geophysical Research Letters*, *39*, L11602. https://doi.org/10.1029/2012GL05202

Grottoli, A. G., & Eakin, C. M. (2007). A review of modern coral $\delta^{18}O$ and $\Delta^{14}C$ proxy records. *Earth-Science Reviews*, *81*(1–2), 67–91. https://doi.org/10.1016/j.earscirev.2006.10.001

Grumet, N. S., Abram, N. J., Beck, J. W., Dunbar, G. B., Gagan, M. K., Guilderson, T. P., Hantoro, W. S., et al. (2004). Coral radiocarbon records of Indian Ocean water mass mixing and wind-induced upwelling along the coast of Sumatra, Indonesia. *Journal of Geophysical Research*, *109*, C05003. https://doi.org/10.1029/2003JC002087

Guilderson, T. P., Fallon, S., Moore, M. D., Schrag, D. P., & Charles, C. D. (2009). Seasonally resolved surface water $\Delta^{14}C$ variability in the Lombok Strait: A coralline perspective. *Journal of Geophysical Research*, *114*, C07029. https://doi.org/10.1029/2008JC004876

Hirabayashi, S., Yokoyama, Y., Suzuki, A., Miyairi, Y., & Aze, T. (2017). Multidecadal oceanographic changes in the western Pacific detected through high-resolution bomb-derived radiocarbon measurements on corals. *Geochemistry, Geophysics, Geosystems*, *18*, 1608–1617. https://doi.org/10.1002/2017GC006854

Hirabayashi, S., Yokoyama, Y., Suzuki, A., Miyairi, Y., Aze, T., Siringan, F., & Maeda, Y. (2017). Radiocarbon variability recorded in coral skeletons from the northwest of Luzon Island, Philippines. *Geoscience Letters*, *4*(1). https://doi.org/10.1186/s40562-017-0081-8

Hsin, Y.-C., Wu, C.-R., & Chao, S.-Y. (2012). An updated examination of the Luzon Strait transport. *Journal of Geophysical Research*, *117*, C03022. https://doi.org/10.1029/2011JC007714

Hu, D., Wu, L., Cai, W., Gupta, A. S., Ganachaud, A., Qiu, B., Gordon, A. L., et al. (2015). Pacific western boundary currents and their roles in climate. *Nature*, *522*(7556), 299–308. http://www.ncbi.nlm.nih.gov/pubmed/26085269. https://doi.org/10.1038/nature14504

Hu, J., Kawamura, H., Hong, H., & Qi, Y. (2000). A review on the currents in the South China Sea: Seasonal circulation, South China Sea Warm Current and Kuroshio Intrusion. *Journal of Oceanography*, *56*(6), 607–624. https://doi.org/10.1023/A:1011117531252

Hua, Q., Barbetti, M., & Rakowski, A. Z. (2013). Atmospheric radiocarbon for the period 1950–2010. *Radiocarbon*, *55*(04), 2059–2072. https://doi.org/10.2458/azu_js_rc.v55i2.16177

Jia, Y., & Chassignet, E. P. (2011). Seasonal variation of eddy shedding from the Kuroshio intrusion in the Luzon Strait. *Journal of Oceanography*, *67*(5), 601–611. https://doi.org/10.1007/s10872-011-0060-1

Jia, Y., & Liu, Q. (2004). Eddy shedding from the Kuroshio bend at Luzon Strait. *Journal of Oceanography*, *60*(6), 1063–1069. https://doi.org/10.1007/s10872-005-0014-6

Jian, Z., Wang, P.-X., Saito, Y., Wang, J., Pflaumann, U., Oba, T., & Cheng, X.-R. (2000). Holocene variability of the Kuroshio Current in the Okinawa Trough, northwestern Pacific Ocean. *Earth and Planetary Science Letters*, *184*(1), 305–319. https://doi.org/10.1016/S0012-821X(00)00321-6

Kalnay, E., Kanamitsu, M., Kistler, R., Collins, W., Deaven, D., Gandin, L., Iredell, M., et al. (1996). The NCEP/NCAR 40-year reanalysis project. *Bulletin of the American Meteorological Society*, *77*(3), 437–471. https://doi.org/10.1175/1520-0477(1996)077<0437:TNYRP>2.0.CO;2

Kim, J.-W., Yeh, S.-W., & Chang, E.-C. (2014). Combined effect of El Niño–Southern Oscillation and Pacific Decadal Oscillation on the East Asian winter monsoon. *Climate Dynamics*, *42*(3-4), 957–971. https://doi.org/10.1007/s00382-013-1730-z

Kim, Y. Y., Qu, T., Jensen, T., Miyama, T., Mitsudera, H., Kang, H.-W., & Ishida, A. (2004). Seasonal and interannual variations of the North Equatorial Current bifurcation in a high-resolution OGCM. *Journal of Geophysical Research*, *109*, C03040. https://doi.org/10.1029/2003JC002013

Lauvset, S. K., Key, R. M., Olsen, A., van Heuven, S., Velo, A., Lin, X., Schirnick, C., et al. (2016). A new global interior ocean mapped climatology: the 1° × 1° GLODAP version 2. *Earth System Science Data*, *8*(2), 325–340.

Lee, H.-J., Chao, S.-Y., & Fan, K.-L. (1999). Flood-ebb disparity of tidally induced recirculation eddies in a semi-enclosed basin: Nan Wan Bay. *Continental Shelf Research*, *19*(7), 871–890. https://doi.org/10.1016/S0278-4343(99)00006-0

Lee, H.-J., Chao, S.-Y., Fan, K.-L., & Kuo, T.-Y. (1999). Tide-induced eddies and upwelling in a semi-enclosed basin: Nan Wan. *Estuarine, Coastal and Shelf Science*, *49*(6), 775–787. https://doi.org/10.1006/ecss.1999.0524

Lee, H.-J., Chao, S.-Y., Fan, K.-L., Wang, Y.-H., & Liang, N.-K. (1997). Tidally induced upwelling in a semi-enclosed basin: Nan Wan Bay. *Journal of Oceanography*, *53*, 467–480.

Levitus, S. (1982). *Climatological Atlas of the World Ocean*. Washington, D. C: U.S. Government Printing Office.

Li, X., Liu, Y., Hsin, Y.-C., Liu, W., Shi, Z., Chiang, H. W., & Shen, C. C. (2017). Coral record of variability in the upstream Kuroshio Current during 1953–2004. *Journal of Geophysical Research: Oceans*, *122*, 6936–6946. https://doi.org/10.1002/2017JC012944

Liang, W.-D., Yang, Y. J., Tang, T. Y., & Chuang, W.-S. (2008). Kuroshio in the Luzon Strait. *Journal of Geophysical Research*, *113*, C08048. https://doi.org/10.1029/2007JC004609

Lien, R.-C., Ma, B., Cheng, Y.-H., Ho, C.-R., Qiu, B., Lee, C. M., & Chang, M.-H. (2014). Modulation of Kuroshio transport by mesoscale eddies at the Luzon Strait entrance. *Journal of Geophysical Research: Oceans*, *119*, 2129–2142. https://doi.org/10.1002/2013JC009548

Liu, J., Li, T., Xiang, R., Chen, M., Yan, W., Chen, Z., & Liu, F. (2013). Influence of the Kuroshio Current intrusion on Holocene environmental transformation in the South China Sea. *The Holocene*, *23*(6), 850–859. https://doi.org/10.1177/0959683612474481

Mahadevan, A. (2001). An analysis of bomb radiocarbon trends in the Pacific. *Marine Chemistry*, *73*(3-4), 273–290. https://doi.org/10.1016/S0304-4203(00)00113-4

Masumoto, Y., Sasaki, H., Kagimoto, T., Komori, N., Ishida, A., Sasai, Y., et al. (2004). A fifty-year eddy-resolving simulation of the world ocean—Preliminary outcomes of OFES (OGCM for the Earth Simulator). *Journal of the Earth Simulator*, *1*, 35–56.

Metzger, E. J., & Hurlburt, H. E. (1996). Coupled dynamics of the South China Sea, the Sulu Sea, and the Pacific Ocean. *Journal of Geophysical Research*, *101*(C5), 12,331–12,352. https://doi.org/10.1029/95JC03861

Metzger, E. J., & Hurlburt, H. E. (2001). The nondeterministic nature of Kuroshio penetration and eddy shedding in the South China Sea. *Journal of Physical Oceanography*, *31*(7), 1712–1732. https://doi.org/10.1175/1520-0485(2001)031<1712:TNNOKP>2.0.CO;2

Mitsuguchi, T., Dang, P. X., Kitagawa, H., Yoneda, M., & Shibata, Y. (2007). Tropical South China Sea surface ^{14}C record in an annually-banded coral. *Radiocarbon*, *49*(02), 905–914. https://doi.org/10.1017/S0033822200042776

Monterey, G., & Levitus, S. (1997). *Seasonal variability of mixed layer depth for the world ocean*. Washington, D. C: U.S. Government Printing Office.

Nan, F., Xue, H., Chai, F., Wang, D., Yu, F., Shi, M., Guo, P., et al. (2013). Weakening of the Kuroshio Intrusion into the South China Sea over the past two decades. *Journal of Climate*, *26*(20), 8097–8110. https://doi.org/10.1175/JCLI-D-12-00315.1

Nan, F., Xue, H., & Yu, F. (2015). Kuroshio intrusion into the South China Sea: A review. *Progress in Oceanography*, *137*, 314–333. https://doi.org/10.1016/j.pocean.2014.05.012

Nan, F., Yu, F., Xue, H., Zeng, L., Wang, D., Yang, S., & Nguyen, K.-C. (2016). Freshening of the upper ocean in the South China Sea since the early 1990s. *Deep Sea Research Part I: Oceanographic Research Papers*, *118*, 20–29. https://doi.org/10.1016/j.dsr.2016.10.010

Ndah, A. B., Dagar, L., & Becek, K. (2017). Multi-temporal patterns of upwelling–downwelling dynamics in the South China Sea based on a 47-year time-series of the NOAA-ERD upwelling index. *Regional Studies in Marine Science*, *16*, 225–239. https://doi.org/10.1016/j.rsma.2017.08.017

Nydal, R. (2000). Radiocarbon in the ocean. *Radiocarbon*, *42*(1), 81–98.

Olsen, A., Key, R. M., van Heuven, S., Lauvset, S. K., Velo, A., Lin, X., Schirnick, C., et al. (2016). The Global Ocean Data Analysis Project version 2 (GLODAPv2)—An internally consistent data product for the world ocean. *Earth System Science Data*, *8*(2), 297–323.

Ostlund, H. G., & Stuiver, M. (1980). GEOSECS Pacific radiocarbon. *Radiocarbon*, *22*(1), 25–53.

Peñaflor, E. L., Villanoy, C. L., Liu, C.-T., & David, L. T. (2007). Detection of monsoonal phytoplankton blooms in Luzon Strait with MODIS data. *Remote Sensing of Environment*, *109*(4), 443–450. https://doi.org/10.1016/j.rse.2007.01.019

Peng, T.-H., Key, R. M., & Ostlund, G. (1998). Temporal variations of bomb radiocarbon inventory in the Pacific Ocean. *Marine Chemistry*, *60*(1-2), 3–13. https://doi.org/10.1016/S0304-4203(97)00089-3

Qiu, B., & Chen, S. (2010). Interannual-to-decadal variability in the bifurcation of the North Equatorial Current off the Philippines. *Journal of Physical Oceanography*, *40*(11), 2525–2538. https://doi.org/10.1175/2010JPO4462.1

Qiu, B., & Lukas, R. (1996). Seasonal and interannual variability of the North Equatorial Current, the Mindanao Current, and the Kuroshio along the Pacific western boundary. *Journal of Geophysical Research*, *101*(C5), 12,315–12,330. https://doi.org/10.1029/95JC03204

Qu, T., Girton, J. B., & Whitehead, J. A. (2006). Deepwater overflow through Luzon Strait. *Journal of Geophysical Research*, *111*, C01002. https://doi.org/10.1029/2005JC003139

Qu, T., Kim, Y. Y., & Yaremchuk, M. (2004). Can Luzon Strait transport play a role in conveying the impact of ENSO to the South China Sea? *Journal of Climate*, *17*(18), 3644–3657. https://doi.org/10.1175/1520-0442(2004)017<3644:CLSTPA>2.0.CO;2

Qu, T., Mitsudera, H., & Yamagata, T. (1998). On the western boundary currents in the Philippine Sea. *Journal of Geophysical Research*, *103*(C4), 7537–7548. https://doi.org/10.1029/98JC00263

Qu, T., Mitsudera, H., & Yamagata, T. (2000). Intrusion of the North Pacific waters into the South China Sea. *Journal of Geophysical Research*, *105*(C3), 6415–6424. https://doi.org/10.1029/1999JC900323

Ramos, R. D., Goodkin, N. F., Siringan, F. P., & Hughen, K. A. (2017). *Diploastrea heliopora* Sr/Ca and $\delta^{18}O$ records from northeast Luzon, Philippines: An assessment of interspecies coral proxy calibrations and climate controls of sea surface temperature and salinity. *Paleoceanography*, *32*, 424–438. https://doi.org/10.1002/2017PA003098

Shaw, P.-T., & Chao, S.-Y. (1994). Surface circulation in the South China Sea. *Deep Sea Research Part I: Oceanographic Research Papers*, *41*(11-12), 1663–1683. https://doi.org/10.1016/0967-0637(94)90067-1

Shaw, P.-T., Chao, S.-Y., Liu, K.-K., Pai, S.-C., & Liu, C.-T. (1996). Winter upwelling off Luzon in the northeastern South China Sea. *Journal of Geophysical Research*, *101*(C7), 16435–16448. https://doi.org/10.1029/96JC01064

Shen, C.-C., Liu, K.-K., Lee, M.-Y., Lee, T., Wang, C.-H., & Lee, H.-J. (2005). A novel method for tracing coastal water masses using Sr/ca ratios and salinity in Nanwan Bay, southern Taiwan. *Estuarine, Coastal and Shelf Science*, *65*(1–2), 135–142. https://doi.org/10.1016/j.ecss.2005.05.010

Southon, J., Santos, G., Druffel-Rodriguez, K., Druffel, E. R. M., Trumbore, S., Xu, X., Griffin, S., et al. (2004). The keck carbon cycle AMS laboratory, University of California, Irvine: Initial operation and a background surprise. *Radiocarbon*, *46*(01), 41–49. https://doi.org/10.1017/S0033822200039333

Stuiver, M., Ostlund, G., & McConnaughey, T. A. (1981). GEOSECS Atlantic and Pacific ^{14}C distribution. In B. Bolin (Ed.), *Carbon cycle modelling, Scientific Committee on Problems of the Environment (SCOPE 16)* (pp. 201–222). New York: John Wiley.

Stuiver, M., & Polach, H. A. (1977). Discussion: Reporting of ^{14}C data. *Radiocarbon*, *19*(03), 355–363. https://doi.org/10.1017/S0033822200003672

Stuiver, M., & Quay, P. D. (1981). Atmospheric ^{14}C changes resulting from fossil fuel CO_2 release and cosmic ray flux variability. *Earth and Planetary Science Letters*, *53*(3), 349–362. https://doi.org/10.1016/0012-821X(81)90040-6

Tian, J., Yang, Q., Liang, X., Xie, L., Hu, D., Wang, F., & Qu, T. (2006). Observation of Luzon Strait transport. *Geophysical Research Letters*, *33*, L19607. https://doi.org/10.1029/2006GL026272

Ujiie, H., & Ujiie, Y. (1999). Late Quaternary course changes of the Kuroshio Current in the Ryukyu Arc region, northwestern Pacific Ocean. *Marine Micropaleontology*, *37*(1), 23–40. https://doi.org/10.1016/S0377-8398(99)00010-9

Wang, L., Chen, W., & Huang, R. (2008). Interdecadal modulation of PDO on the impact of ENSO on East Asian winter monsoon. *Geophysical Research Letters*, *35*, L20702. https://doi.org/10.1029/2005GL035287

Wang, P.-X., & Li, Q. (2009). In P.-X. Wang & Q. Li (Eds.), *The South China Sea: Paleoceanography and sedimentology* (1st ed.). Netherlands: Springer.

Wang, Q.-Y., & Hu, D.-X. (2006). Bifurcation of the North Equatorial Current derived from altimetry in the Pacific Ocean. *Journal of Hydrodynamics, Series B*, *18*(5), 620–626.

Wu, C.-R. (2013). Interannual modulation of the Pacific Decadal Oscillation (PDO) on the low-latitude western North Pacific. *Progress in Oceanography*, *110*, 49–58. https://doi.org/10.1016/j.pocean.2012.12.001

Wu, C.-R., Wang, Y.-L., Lin, Y.-F., Chiang, T.-L., & Wu, C.-C. (2016). Weakening of the Kuroshio Intrusion into the South China Sea under the global warming hiatus. *IEEE Journal of Selected Topics in Applied Earth Observations and Remote Sensing*, *9*(11), 5064–5070. https://doi.org/10.1109/JSTARS.2016.2574941

Wyrtki, K. (1961). *Physical oceanography of the Southeast Asian Waters* (Vol. 2). La Jolla, California: Scripps Institution of Oceanography.

Xu, X., Trumbore, S. E., Zheng, S., Southon, J. R., McDuffee, K. E., Luttgen, M., & Liu, J. C. (2007). Modifying a sealed tube zinc reduction method for preparation of AMS graphite targets: Reducing background and attaining high precision. *Nuclear Instruments and Methods in Physics Research Section B: Beam Interactions with Materials and Atoms*, *259*(1), 320–329. https://doi.org/10.1016/j.nimb.2007.01.175

Xue, H., Chai, F., Pettigrew, N., Xu, D., Shi, M., & Xu, J. (2004). Kuroshio intrusion and the circulation in the South China Sea. *Journal of Geophysical Research*, *109*, C02017. https://doi.org/10.1029/2002JC001724

Yamazaki, A., Watanabe, T., Tsunogai, U., Iwase, F., & Yamano, H. (2016). A 150-year variation of the Kuroshio transport inferred from coral nitrogen isotope signature. *Paleoceanography*, *31*, 838–846. https://doi.org/10.1002/2015PA002880

Yang, Q., Tian, J., & Zhao, W. (2010). Observation of Luzon Strait transport in summer 2007. *Deep Sea Research Part I: Oceanographic Research Papers*, *57*(5), 670–676. https://doi.org/10.1016/j.dsr.2010.02.004

Yaremchuk, M., & Qu, T. (2004). Seasonal variability of the large-scale currents near the coast of the Philippines. *Journal of Physical Oceanography*, *34*(4), 844–855. https://doi.org/10.1175/1520-0485(2004)034<0844:SVOTLC>2.0.CO;2